# 4D Pulse Wave Imaging with sub aperture compounding in the carotid artery in simulations, phantoms and human subjects


Nirvedh H. Meshram
Department of Biomedical Engineering
Columbia University
New York, USA
nhm2119@columbia.edu

Julien Grondin
Department of Radiology
Columbia University
New York, USA
jlg2216@columbia.edu

Grigorios Marios Karageorgos
Department of Biomedical Engineering
Columbia University
New York, USA
gk2490@columbia.edu

Rachel Weber
Department of Biomedical Engineering
Columbia University
New York, USA
rw2727@columbia.edu

Elisa E. Konofagou
Department of Biomedical Engineering
Department of Radiology
Columbia University
New York, USA
ek2191@columbia.edu



***Abstract*- Pulse Wave Imaging (PWI) can non-invasively and regionally map and quantify local pulse wave velocities (PWV). Assumptions regarding axis symmetry are intrinsic to 2D imaging. 3D imaging can provide an added advantage especially in pathological arteries where radial symmetry does not hold. Previously a 3D feasibility was presented for pulse wave imaging with a narrow field of view in vivo using plane wave imaging. In this study, we expanded the field of view compared to the previous method by using diverging waves and improve the imaging quality by using coherent compounding. We demonstrated agreement in simulations and PVA phantoms. Initial *in vivo* results in a human patient with stenotic carotid arteries are also presented. 3D PWI can thus be used in conjunction with diverging wave imaging to provide sufficient fields of view for clinical PWI.**



Keywords— **2D array transducer, 3D ultrasound imaging, high frame rate imaging, pulse wave imaging,**


## I. Introduction

Stenosis in carotid arteries caused by plaque buildup is a leading cause of atherosclerosis, which can cause ischemic strokes[1]. It is known that plaque composition and structure play a role in the probability of plaque rupture leading to stroke. However, the current clinical standard of care is based on percentage of stenosis alone [2-4].

An important mechanical property for the carotid artery walls and plaques is stiffness. Several ultrasound-based methods have been developed for quantifying carotid stiffness. These include vascular elastography[5-7], acoustic radiation force imaging(ARFI)[8-10], shear wave elastography[11-14] and pulse wave imaging (PWI) [15-19].

PWI is a non-invasive technique that maps pulse wave velocity (PWV) which is a surrogate measure for stiffness. PWI has been optimized for high frame rating imaging using plane wave image compounding)[15-19]. Piecewise PWI (pPWI) was also implemented by our group which enabled imaging and tracking of pulse wave propagation along few mm of artery wall[15]. However, fixed segment placement in pPWI resulted in segments spanning across inhomogeneous arterial segment compromising the PWV values due to non-linear pulse propagation. Recently, this was solved by adaptive PWI[18] that enabled automated partitioning of heterogeneous arterial segment.

PWI maps the propagation of pulse in 2D. Imaging of a 3D phenomenon in 2D has its limitation. It is assumed the wave propagation direction is parallel to the imaging plane. This is not necessarily true given the tortuosity and branching of the arteries and can lead to erroneous PWV estimation. Moreover, isotropy around the axis of the artery is assumed for pulse propagation and arterial wall displacement. While this is a reasonable assumption in healthy arteries, in pathological arteries this is not true and can lead to erroneous PWV estimation. A 3D PWI estimation method can alleviate these problems. An initial 3D PWI method was demonstrated by our group[20] in silicone phantoms and healthy human volunteers. The method used plane wave imaging with a 16x16 matrix array transducer without compounding. The lateral and elevational field of view was limited to the aperture of the transducer which was 13.6 mm x 13.6 mm.

In this study, we use a 32x32 matrix array transducer with diverging waves to have a larger field of view. We will also demonstrate initial feasibility in a patient with stenotic carotid artery. Furthermore, we employ a coherent wave compounding that improves image quality and has been used for 3D cardiac elastography by our group [21].

## II. Methods

### A. Configuration of Ultrasound System

The ultrasound transducer used in this paper was a 2D array with 32x32 elements. The inter-element spacing (pitch) was 0.3 mm and center frequency was 3MHz (Vermon SA, France). Four Verasonics Vantage systems (Vantage, Verasonics, Kirkland, WA) with 256 transmit/receive channels each were synchronized to drive the transducer[22]. The acquisition depth was set to 40mm and a pulse repletion frequency (prf) was 14000 Hz. In this paper, we utilized coherent diverging wave compounding with virtual sources arranged in a 3x3 grid to make an imaging sector of 72 degrees

in both the lateral and elevational direction. Thus, the volume rate was 14000/9 Hz which is 1555 Hz.

2D high frame rate imaging was also performed to validate the 3D approach. A linear array transducer with 128 elements and center frequency of 5 MHz and a 60% bandwidth (L7-4, ATL Ultrasound, Bothell, WA, USA) was used. A coherent compounding acquisition sequence with 5 plane waves at angle increments of 1 degree. The PRF of the acquisition was 8333Hz. A Verasonics Vantage 256 system (Verasonics, Kirkland, USA) was used to make the acquisition.

### *B. Simulation Study*

A 50 mm tube with 10 mm diameter and 0.5 mm thickness was simulated in Field II[23]. The axis of the tube was at 20 mm depth. A sinusoidal pulse with a 4 m/s propagation velocity and peak radial wall velocity of 5 mm/s was propagated through the tube. Temporal resolution of the simulation input was equal to 1/PRF of the acquisition setup. Same acquisition parameters described in the previous section were used to generate the simulated data.

### *C. Phantom Study*

A longitudinal vessel phantom was designed using Polyvinyl alcohol (PVA) material following the work of Chee et al. (2016) and Galluzzo et al. (2015)[24, 25]. The vessel mimicking mixture consisted of (by weight), 78% distilled water, 10% PVA powder (Sigma-Aldrich, St. Louis, MO, USA), 10% glycerol, to increase the sound speed and 2% of graphite acoustic scatters (Sigma-Aldrich). The mixture was continuously stirred at 90°C for approximately 25 minutes, after which it was left cooling and degassed. It was then poured in a coaxial cylindrical mold. The outer vessel diameter was 12 mm and thickness was 2 mm. The material filled mold was then put through 6 freeze thaw cycles where it was frozen at -20 $^0$C for 12 hours and thawed at room temperature for 12 hours. After 6 days the phantoms were mounted on a custom scaffold and space in the scaffold was filled with porcine skin gelatin to stabilize the phantom and to mimic the neck muscle surrounding the artery.

A programmable pump (CompuFlow 1000, Shelley Medical Imaging Technologies, Toronto, Canada) filled with blood mimicking fluid[26] was connected to the phantom. A physiological pulse[27] with a minimum flow of 0.05 ml/s (base human flow) and a maximum peak of 0.2 ml/s (max systole) with a duration of 0.4 s. A total duration of 1.9 s was provided between pulses to allow dissipation of reflection waves.

### *D. Human Study*

A 76-year-old male with 40% stenosis in his right carotid artery underwent 3D and 2D ultrasound imaging with the acquisition protocol described previously on the right common carotid artery (CCA) and right internal carotid artery (ICA). The study was approved by the Human Research Protection Office (HRPO) and Institutional Review Boards (IRBs) of Columbia University (protocol AAAR0022).

### *E. Pulse Wave Estimation*

Delay and sum beamforming was performed in parallel using GPU acceleration in CUDA. Axial displacement was computed using 2D normalized cross correlation[28] and 1D search with cosine subsample interpolation on beamformed RF data. Scan converted B-mode and axial displacements were then obtained in the Cartesian co-ordinate system. Cross-sectional images of the artery were then manually segmented slice by slice to form a complete segmentation of the artery.

Low pass filtering with a Butterworth filter were performed on the displacement values at the segmentation points was performed in the time dimension. The low-pass filter limit was 100 Hz with a 3dB attenuation at 150 Hz. The axial displacements were then unit converted to axial wall velocities. Posterior wall velocities were pointwise subtracted from anterior wall velocities to cancel global wall motion to generate a spatiotemporal map over a cardiac cycle. Fifty percent upstroke markers on the spatiotemporal map were calculated and fitted to a plane using robust least square fitting. PWV was calculated as the slope of the plane.

For 2D estimation followed the same process of calculating 50% upstroke markers along the long axis of the artery. A line was fitted through the markers using linear regression. PWV was calculated as the slope of the line.

## III. RESULTS

### *A. Simulation Results*

Figure 1(a) presents a 3D B-mode from the simulation dataset. Fig. 1(b) presents a plane fit through 50% upstroke markers for the simulation dataset. A time progression of the estimated axial wall velocities is presented in Fig 1(c) and 1(d). The calculated PWV was 3.98 m/s ($R^2$=0.99). The ground truth PWV was 4 m/s. Fig. 2 presents longitudinal and transverse slice with single full aperture diverging wave in Fig. 2(a) and 2(b) and the corresponding slices with sub aperture diverging wave coherent compounding method used in this paper with 9 virtual sources in 2(c) and 2(d).

### *B. Phantom Results*

2D B-mode with the L7-4 transducer with the upper and lower wall segmentation and a 3D B-mode from the 32x32 matrix array for the phantom are presented in Fig. 3(a) and 3(b) respectively. The spatiotemporal map with pulse wave fitting is presented in Fig. 3(c) with the 2D method. The surface fitting through 50% upstroke markers for the 3D method is presented in Fig. 3(d). A PWV of 2.66 m/s ($R^2$=0.97) with the 2D method and 2.71 m/s ($R^2$=0.86) with the 3D method was calculated

### *C. In vivo Results*

Fig. 4(a) presents the 2D B-mode image of the right ICA. Fig. 4(b) presents the corresponding transverse slice from 3D imaging that best shows the plaque region. The spatiotemporal map with pulse wave fitting is presented in Fig.4(c) with the 2D method. The surface fitting through 50% upstroke markers for the 3D method is presented in Fig.4(d). A PWV of 5.23 m/s ($R^2$=0.28) with the 2D method and 2.21 m/s ($R^2$=0.48) with the 3D method was calculated in the ICA. For the CCA, a PWV of 5.66 m/s ($R^2$=0.92) with the 2D method and 4.86 m/s ($R^2$=0.86) with the 3D method was calculated.

## IV. CONCLUSION

Coherent diverging wave compounding with a 32x32 matrix array transducer improved image quality and field of view

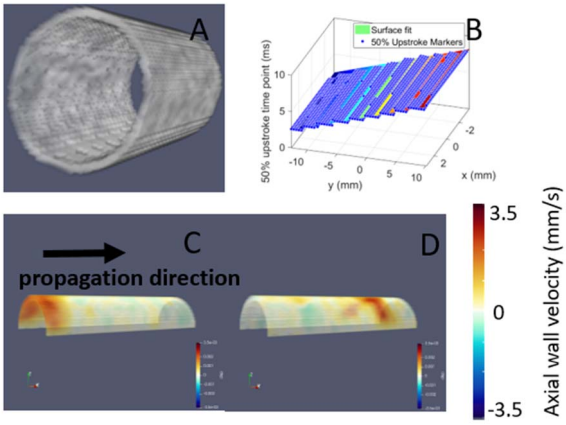


Figure 1: Simulation results (a) 3D B-mode of simulated tube (b) Surface fit through 50% upstroke markers (c) Axial Wall velocities at t = 3.2 ms (d) Axial Wall velocities at t = 7.7 ms

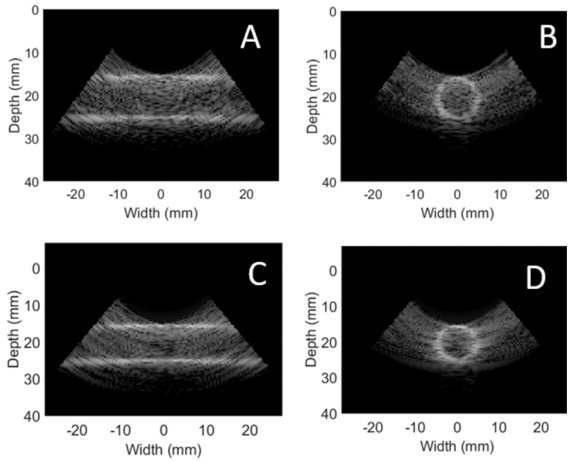


Figure 2: Improvement in field of view and resolution with full aperture single diverging wave: (a) longitudinal slice (b) transverse slice and sub aperture diverging wave coherent compounding with 9 sources: (c) longitudinal slice (d) transverse slice

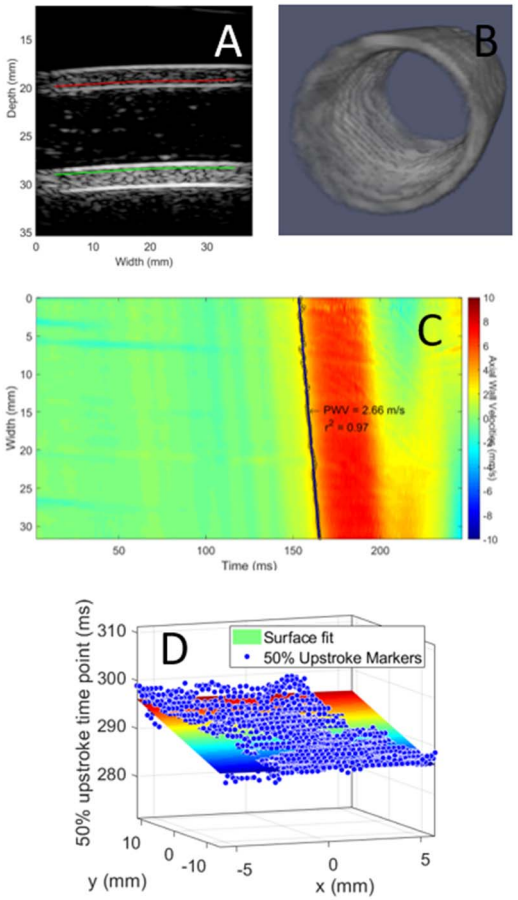


Figure 3: Phantom results (a) 2D B-mode (b) 3D B-mode (c) Spatiotemporal map (2D method) (d) Surface fit through 50% upstroke markers

(Fig. 2) that enabled 4D pulse wave imaging in the stenotic human arteries. The method was validated against a 2D approach in phantoms and demonstrated good agreement. Agreement was also observed in a stenotic CCA. Feasibility in stenotic

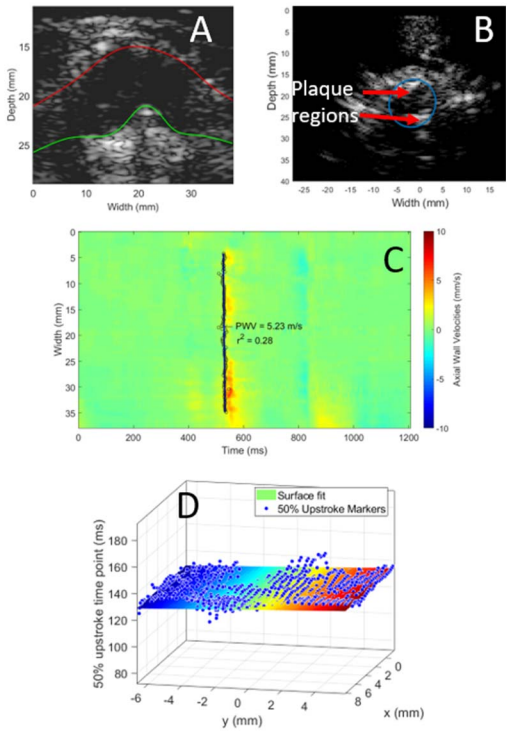


Figure 4: In vivo results (a) 2D B-mode of ICA (b) Transverse slice from 3D B-mode showing the same plaque regions (c) Spatiotemporal map (2D method) (d) Surface fit through 50% upstroke markers

ICA was also demonstrated but agreement with 2D approach was lower due to imaging challenges.

ACKNOWLEDGEMENTS

The study was funded in part by the National Institutes of Health: NIH R01-HL135734.

REFERENCES


[1] P. Libby, P. M. Ridker, and G. K. Hansson, "Progress and challenges in translating the biology of atherosclerosis," *Nature,* vol. 473, no. 7347, pp. 317-325, 2011.

[2] M. Naghavi *et al.*, "From vulnerable plaque to vulnerable patient: a call for new definitions and risk assessment strategies: Part I," *Circulation,* vol. 108, no. 14, pp. 1664-1672, 2003.

[3] L. Saba *et al.*, "Imaging of the carotid artery vulnerable plaque," *Cardiovasc. Intervent. Radiol.,* vol. 37, no. 3, pp. 572-585, 2014.

[4] R. J. Dempsey *et al.*, "Carotid atherosclerotic plaque instability and cognition determined by ultrasound-measured plaque strain in asymptomatic patients with significant stenosis," *J. Neurosurg.,* vol. 128, no. 1, pp. 111-119, 2018.

[5] H. Hansen, G. De Borst, M. Bots, F. Moll, G. Pasterkamp, and C. De Korte, "Noninvasive compound ultrasound elastography for vulnerable plaque detection: in vivo validation," *Eur. Heart J.,* vol. 34, no. suppl_1, 2013.

[6] R. Nayak *et al.*, "Principal strain vascular elastography: Simulation and preliminary clinical evaluation," *Ultrasound Med. Biol.,* vol. 43, no. 3, pp. 682-699, 2017.

[7] N. H. Meshram *et al.*, "Quantification of carotid artery plaque stability with multiple region of interest based ultrasound strain indices and relationship with cognition," *Phys. Med. Biol.,* vol. 62, no. 15, pp. 6341-6360, Jul 17 2017, doi: 10.1088/1361-6560/aa781f.

[8] D. Dumont, R. H. Behler, T. C. Nichols, E. P. Merricks, and C. M. Gallippi, "ARFI imaging for noninvasive material characterization of atherosclerosis," *Ultrasound Med. Biol.,* vol. 32, no. 11, pp. 1703-1711, 2006.

[9] T. J. Czernuszewicz *et al.*, "Non-invasive in vivo characterization of human carotid plaques with acoustic radiation force impulse ultrasound: Comparison with histology after endarterectomy," *Ultrasound Med. Biol.,* vol. 41, no. 3, pp. 685-697, 2015.

[10] G. Torres, T. J. Czernuszewicz, J. W. Homeister, M. A. Farber, M. C. Caughey, and C. M. Gallippi, "Carotid Plaque Fibrous Cap Thickness Measurement by ARFI Variance of Acceleration: In Vivo Human Results," *IEEE Trans. Med. Imaging,* 2020.

[11] J. Garrard *et al.*, "Shear Wave Elastography May Be Superior to Greyscale Median for the Identification of Carotid Plaque Vulnerability: A Comparison with Histology," *Ultraschall in der Medizin-European Journal of Ultrasound,* vol. 36, no. 04, pp. 386-390, 2015.

[12] E. Widman, E. Maksuti, C. Amador, M. W. Urban, K. Caidahl, and M. Larsson, "Shear wave elastography quantifies stiffness in Ex vivo porcine artery with stiffened arterial region," *Ultrasound Med. Biol.,* vol. 42, no. 10, pp. 2423-2435, 2016.

[13] Y. Majdouline *et al.*, "Endovascular shear strain elastography for the detection and characterization of the severity of atherosclerotic plaques: In vitro validation and in vivo evaluation," *Ultrasound Med. Biol.,* vol. 40, no. 5, pp. 890-903, 2014.

[14] K. V. Ramnarine, J. W. Garrard, B. Kanber, S. Nduwayo, T. C. Hartshorne, and T. G. Robinson, "Shear wave elastography imaging of carotid plaques: feasible, reproducible and of clinical potential," *Cardiovasc. Ultrasound,* vol. 12, no. 1, p. 1, 2014.

[15] I. Z. Apostolakis, S. D. Nandlall, and E. E. Konofagou, "Piecewise pulse wave imaging (pPWI) for detection and monitoring of focal vascular disease in murine aortas and carotids in vivo," *IEEE Trans. Med. Imaging,* vol. 35, no. 1, pp. 13-28, 2016.

[16] I. Z. Apostolakis, G. M. Karageorgos, P. Nauleau, S. D. Nandlall, and E. E. Konofagou, "Adaptive Pulse Wave Imaging: automated spatial vessel wall inhomogeneity detection in phantoms and in-vivo," *IEEE Trans. Med. Imaging,* 2019.

[17] G. M. Karageorgos *et al.*, "Arterial wall mechanical inhomogeneity detection and atherosclerotic plaque characterization using high frame rate pulse wave imaging in carotid artery disease patients in vivo," *Phys. Med. Biol.,* vol. 65, no. 2, p. 025010, 2020.

[18] I. Apostolakis, G. Karageorgos, P. Nauleau, S. Nandlall, and E. Konofagou, "Adaptive Pulse Wave Imaging: Automated Spatial Vessel Wall Inhomogeneity Detection in Phantoms and in-Vivo," *IEEE Trans. Med. Imaging,* vol. 39, no. 1, p. 259, 2020.

[19] R. X. Li *et al.*, "Pulse Wave Imaging in Carotid Artery Stenosis Human Patients in Vivo," *Ultrasound Med. Biol.,* vol. 45, no. 2, pp. 353-366, 2019.

[20] I.-Z. Apostolakis, P. Nauleau, C. Papadacci, M. D. McGarry, and E. E. Konofagou, "Feasibility and validation of 4-D pulse wave imaging in phantoms and in vivo," *IEEE transactions on ultrasonics, ferroelectrics, and frequency control,* vol. 64, no. 9, pp. 1305-1317, 2017.

[21] J. Grondin and E. E. Konofagou, "3D Myocardial Elastography with Coherent Compounding of Diverging Waves," *IEEE International Ultrasonics Symposium,* 2019.

[22] J. Grondin, D. Wang, C. S. Grubb, N. Trayanova, and E. E. Konofagou, "4D cardiac electromechanical activation imaging," *Comput. Biol. Med.,* vol. 113, p. 103382, 2019.

[23] J. A. Jensen, "Simulation of advanced ultrasound systems using Field II," in *2004 2nd IEEE International Symposium on Biomedical Imaging: Nano to Macro (IEEE Cat No. 04EX821)*, 2004: IEEE, pp. 636-639.

[24] A. J. Chee, C. K. Ho, B. Y. Yiu, and C. Alfred, "Walled carotid bifurcation phantoms for imaging investigations of vessel wall motion and blood flow dynamics," *IEEE transactions on ultrasonics, ferroelectrics, and frequency control,* vol. 63, no. 11, pp. 1852-1864, 2016.

[25] F. Galluzzo, F. Leonardo, A. Ceruti, L. De Marchi, and C. Corsi, "Design of anthropomorphic atherosclerotic carotid artery flow phantoms for ultrasound images," in *2015 Computing in Cardiology Conference (CinC)*, 2015: IEEE, pp. 721-724.

[26] D. Holdsworth, D. Rickey, M. Drangova, D. Miller, and A. Fenster, "Computer-controlled positive displacement pump for physiological flow simulation," *Med. Biol. Eng. Comput.,* vol. 29, no. 6, pp. 565-570, 1991.

[27] K. Taylor, "Clinical applications of carotid Doppler ultrasound," *Clinical applications of doppler ultrasound,* pp. 120-161, 1988.

[28] N. H. Meshram and T. Varghese, "GPU Accelerated Multilevel Lagrangian Carotid Strain Imaging," *IEEE Transactions on Ultrasonics, Ferroelectrics, and Frequency Control,* vol. 65, no. 8, pp. 1370-1379, 2018.